Can bars be destroyed by a central mass concentration? I. Simulations

E. Athanassoula, J. C. Lambert, W. Dehnen

Mon. Not. R. Astron. Soc. **363,** 496–508 (2005) doi:10.1111/j.1365-2966.2005.09445.x

Can bars be destroyed by a central mass concentration? – I. Simulations

E. Athanassoula,[1]★ J. C. Lambert[1] and W. Dehnen[2]
[1]*Observatoire de Marseille, 2 Place Le Verrier, F-13248 Marseille Cedex 4, France*
[2]*Department of Physics and Astronomy, University of Leicester, Leicester LEI 7RH*

Accepted 2005 July 18. Received 2005 June 23; in original form 2005 February 10

ABSTRACT

We study the effect of a central mass concentration (CMC) on the secular evolution of a barred disc galaxy. Unlike previous studies, we use fully self-consistent 3D *N*-body simulations with live haloes, which are known to be important for bar evolution. The CMC is introduced gradually, to avoid transients. In all cases for which the mass of the CMC is of the order of, or more than, a few per cent of the mass of the disc, the strength of the bar decreases noticeably. The amount of this decrease depends strongly on the bar type. For a given CMC, bars with an exponential surface-density profile, which formed in a disc-dominated galaxy (MD-type bars), can be totally destroyed, while strong bars with a flat surface-density profile, whose evolution is significantly affected by the halo (MH-type bars), witness only a decrease of their strength. This decrease occurs simultaneously from both the innermost and outermost parts of the bar. The CMC has a stronger effect on the Fourier components of higher azimuthal wavenumber *m*, leading to fatter and/or less rectangular bars. Furthermore, the CMC changes the side-on outline from peanut-shaped to boxy or, for massive CMCs, to elliptical. Similarly, side-on initially boxy outlines can be destroyed. The CMC also influences the velocity dispersion profiles. Most of the decrease of the bar strength occurs while the mass of the CMC increases, and it is accompanied by an increase of the pattern speed. In all our simulations, the mass of the CMC necessary in order to destroy the bar is at least several per cent of the mass of the disc. This argues that observed supermassive black holes are not likely to destroy pre-existing bars.

Key words: methods: *N*-body simulations – galaxies: bulges – galaxies: evolution – galaxies: kinematics and dynamics – galaxies: structure.

1 INTRODUCTION

Both bars and central mass concentrations (hereafter CMCs) are features that are present in the majority of disc galaxies. Thus, bars harbouring a CMC should be the rule rather than the exception, and it is important to study the effects of the latter on the evolution of the former (and vice versa). Observations in near-infrared wavelengths, where the effect of dust is largely suppressed, reveal that between 70 and 90 per cent of all disc galaxies have a bar component (Seigar & James 1998; Eskridge et al. 2000; Grosbøl, Patsis & Pompei 2004). CMCs – such as massive black holes, central discs, dense central stellar clusters – are very frequent, too.

Supermassive black holes have a mass of the order of 10^6 – 10^9 $M_\odot$, which correlates with the luminosity, the mass, and, in particular, the velocity dispersion of the hosting bulge (Kormendy & Richstone 1995; Magorrian et al. 1998; Ferrarese & Merritt 2000; Gebhardt et al. 2000; Tremaine et al. 2002; McLure & Dunlop 2002; Marconi & Hunt 2003). Such correlations lead to a ratio of supermassive black hole mass to bulge mass of the order of 10^{-3} (see also Kormendy & Gebhardt 2001). The mass of the CMC is in fact larger than that of the black hole, since the black hole pulls inwards the bulge and disc material in its immediate neighbourhood and thus forms a cusp, which contributes to the CMC mass (Peebles 1972; Shapiro & Lightman 1976; Bahcall & Wolf 1976; Young 1980; Goodman & Binney 1984; Quinlan, Hernquist & Sigurdsson 1995; Leeuwin & Athanassoula 2000).

Compact massive central discs, stellar and/or gaseous, are also examples of CMCs. Gaseous such discs are expected to form particularly frequently in barred galaxies, as a result of the gas inflow driven by the bar (Athanassoula 1992b; Wada & Habe 1992, 1995; Friedli & Benz 1993; Heller & Shlosman 1994; Regan & Teuben 2004). Indeed, observations have shown that large concentrations of molecular gas can be found in many disc galaxies, and particularly in barred ones (Sakamoto et al. 1999; Regan et al. 2001; Helfer et al. 2003). The mass of such components is of the order of 10^7–10^9 $M_\odot$, while their radial extent varies from several tens of parsecs to a couple of kiloparsecs. Discy bulges (Athanassoula 2005b) are examples of mainly stellar such discs (Kormendy & Kennicutt 2004, and references therein). CMCs can also be central dense stellar clusters, with masses of 10^6–10^8 $M_\odot$.

★E-mail: lia@oamp.fr

Orbital-structure studies, aimed at understanding the effect of the CMC on the bar-supporting orbits, were made first in two dimensions (Hasan & Norman 1990) and then extended to three dimensions (Hasan, Pfenniger & Norman 1993). They include the calculation of the main families of periodic orbits and of their stability. The latter is particularly important, since stable periodic orbits trap around them regular orbits, while unstable periodic orbits generate chaos. These studies showed that with increasing CMC mass or concentration the unstable fraction of the bar-supporting orbits increases, reducing the possibility for barred equilibria.

Orbital-structure studies have thus provided the first crucial step in our understanding of the effect of a CMC on a bar by revealing the mechanism by which a CMC could destroy a bar. These studies can inform us whether a given bar model (i.e. density profile and pattern speed) can coexist with a given CMC. However, the parameter space of bar models is huge and an extensive exploration is neither possible nor meaningful, because nothing will be learned about the *evolution* of a given bar in the presence of a growing CMC.

Such information can only be achieved by appropriate *N*-body simulations, which were pioneered by Norman, Sellwood & Hasan (1996) (hereafter NSH). These authors used particles on a grid to represent the (barred) disc, which was exposed to the gravitational field of the CMC and of a spheroidal (bulge-like) component. For both 2D and 3D simulations, NSH found that a CMC of mass 5 per cent of that of the galaxy is sufficient for bar dissolution. In the *N*-body simulations of Shen & Sellwood (2004) (hereafter SS) the disc is represented by particles on a 3D cylindrical polar grid and, similarly to in NSH, exposed to the gravity of the CMC and of a rigid spherical halo component. These authors found that a CMC mass of a few per cent is necessary to destroy the bar – by and large consistent with the results of NSH. More precisely, in the models displayed in their fig. 5, a CMC mass of approximately 4 per cent that of the disc was necessary for a hard (compact) CMC and of more than 10 per cent for a soft (extended) CMC. They compared two models with different bar strengths and concluded that the strength of the bar hardly influences these numbers.

Recently, Hozumi & Hernquist (1998, 1999, 2005) (hereafter HH) re-examined the problem, solving the Poisson equation by expanding the density and the potential in a set of bi-orthonormal basis functions. Their approach is 2D, which implies the necessity for a rigid halo potential, as in NSH and SS. These authors find that a CMC of mass 0.5 per cent of the disc mass is sufficient to destroy the bar. Thus, their limiting CMC mass is an order of magnitude lower than that given by NSH. The difference between their results and those of NSH and SS is surely significant. Indeed, if the mass necessary to destroy a bar is as small as that claimed by HH, then the masses of CMCs observed in disc galaxies are sufficient to dissolve observed bars on relatively short time-scales. The reverse is true if the NSH and SS picture is correct.

This disagreement between previous studies, as well as their lack of realism in modelling galactic haloes, prompted us to revisit the problem. HH argued that the differences between the two sets of simulations are a result of the different initial density distributions in the disc, since they use an exponential disc, while NSH and SS employ a Kuzmin–Toomre disc (Kuzmin 1956; Toomre 1963). HH argue that, since the latter is more centrally concentrated than the former, the CMC could influence a larger fraction of the disc mass and thus achieve bar dissolution more easily. However, preliminary simulations (Athanassoula, Dehnen & Lambert 2005) showed that bars are rather robust, and so we opted for an exponential disc model that is known to represent well the observed light distribution of disc galaxies (Freeman 1970). This may give the CMC a better chance to destroy the bar, and allows us to check whether indeed the initial density distribution in the disc is of crucial importance for the result. We employ a Poisson solver different from both types previously used in this problem, namely a tree code described in Section 2.2.

Unlike the previous studies, we use a live halo in our simulations, which makes them *fully* self-consistent. This has been shown to be essential for bar formation in the presence of a strong halo component. Indeed, Athanassoula (2002) (hereafter A02) compared two simulations with initially identical disc components and haloes of identical mass distribution. In one case the halo was rigid (represented as an imposed spherical potential) and in the other it was composed of about 10^6 particles. The difference between the evolution in the two cases is stunning (fig. 1 of A02). In the first case, the disc formed only a minor oval confined to the centremost parts of the disc, while in the second case it grew a strong bar with very realistic observed properties (Athanassoula & Misiriotis 2002, hereafter AM02). This important difference is a result of the fact that the angular momentum absorption by the halo is artificially suppressed in one of the two cases, while in the other it is allowed to take place freely (for a comprehensive discussion of the effect of the halo on the angular momentum exchange see Athanassoula 2003, hereafter A03).

The paper is organized as follows. In Section 2 we present our numerical methods and our simulations. Sections 3 and 4 describe the evolution before and after the introduction of the CMC, respectively. We discuss our results and conclude in Section 5.

2 *N*-BODY SIMULATIONS

We first follow the formation and evolution of a bar in two bar-unstable discs. We choose a time after the initial fast bar formation period and during the phase of slow secular evolution. At this time we start growing a CMC in the centre of the disc. The various steps in this work are described in the following subsections.

2.1 Initial conditions

The models are composed of a disc and a halo component. The disc has an initial volume density profile

$$\rho_{\rm d}(R,z) = \frac{M_{\rm d}}{4\pi R_{\rm d}^2 z_0}\ \exp(-R/R_{\rm d})\ {\rm sech}^2(z/z_0), \tag{1}$$

where R is the cylindrical radius, $M_{\rm d}$ is the disc mass, and $R_{\rm d}$ and z_0 are the disc radial and vertical scalelengths, respectively[1]. The initial halo density profile is

$$\rho_{\rm h}(r) = \frac{M_{\rm h}}{2\pi^{3/2}}\ \frac{\alpha}{r_{\rm c}}\ \frac{\exp\left(-r^2/r_{\rm c}^2\right)}{r^2+\gamma^2}, \tag{2}$$

where r is the radius, $M_{\rm h}$ is the halo mass and γ and $r_{\rm c}$ are the halo scalelengths. The former can be considered as the core radius of the halo. The constant α is defined by

$$\alpha = [1 - \sqrt{\pi}\, q\ \exp(q^2)\,(1-{\rm erf}(q))]^{-1}, \tag{3}$$

where $q = \gamma/r_{\rm c}$ (Hernquist 1993). Information on how the initial conditions were set up can be found in Hernquist (1993) and AM02. Both simulations have $M_{\rm d}=1$, $R_{\rm d}=1$, $z_0=0.2$, $M_{\rm h}=5$ and $r_{\rm c}=10$. The first one has a halo with a small core ($\gamma=0.5$) and is thus, following the definition of AM02, MH-type. The second one has a halo with a large core ($\gamma=5$) and is thus of MD-type (AM02). The discs of the two simulations have $Q=1.4$ and 1, respectively, where Q is the stability parameter introduced by Toomre (1964).

[1] The system of coordinates is taken according to the usual convention that the x- and y-axes are on the disc equatorial plane and the z-axis is perpendicular to that plane. In all figures the bar will be along the y-axis.

Our model units of mass and length are simply the disc mass and disc scalelength. In order to convert them to $M_\odot$ and kpc, we need to set the units of length and mass to values representative of the object in consideration, namely a barred galaxy. AM02 used a length unit of 3.5 kpc and a mass unit of $5 \times 10^{10}\,M_\odot$. With $G = 1$, this implies that the model unit of velocity is 248 km s^{-1} and the model unit of time is 1.4×10^7 yr. Thus, time 400 corresponds to 5.6×10^9 yr. This choice, however, is in no way unique, and we can choose different values. For example, we can use a smaller length unit since the scalelength of the disc increases with time (O'Neill & Dubinski 2003; Valenzuela & Klypin 2003) and thus the initial length unit could be chosen to be 2 kpc. Because of this rather wide range of possibilities, we will restrict ourselves to model units and leave it to the readers to convert units according to their needs.

2.2 *N*-body simulations

For the simulations described in this paper, we used the publicly available *N*-body code GYRFALCON, which employs the tree-based force solver FALCON (Dehnen 2000a, 2002). Unlike the standard Barnes & Hut (1986) tree code, which has complexity $\mathcal{O}(N \log N)$, FALCON uses cell–cell interactions, has complexity $\mathcal{O}(N)$, and is about 10 times faster at comparable accuracy. Some of the simulations were run with a proprietary version of the code, which uses the SSE[2] instruction set supported on X86 chips. These instructions allow a substantial speed-up for the computation of body–body forces via direct summation. This method is used within and between small cells and results in a gain of a factor of $\sim$2 for this part of the code. The total gain for the force computation for $N \sim 10^6$ bodies (including the tree build) is about 25 per cent.

In all *N*-body simulations it is necessary to use a softening kernel in order to avoid excessive noise and diverging forces. A Plummer (1911) softening, which has a density kernel $\propto (\varepsilon^2 + r^2)^{-5/2}$, has been used in most simulations made so far. This, however, has the disadvantage that the softened force converges relatively slowly to the Newtonian force (Athanassoula et al. 2000; Dehnen 2001), although the difference becomes negligible, and beyond any numerical importance, at large radii. Here we adopt a softening with a density kernel $\propto(\varepsilon^2 + r^2)^{-7/2}$ (Dehnen et al. 2004), which converges much faster to the accurate Newtonian force. This is particularly interesting for the problem at hand, as will be discussed in the final section. We adopted a softening length ε of 0.03, which corresponds roughly to a Plummer softening length of 0.02 (in the sense that the maximum two-body force is the same). A small softening length is useful in this problem, since the CMC will create an increased central concentration of the disc and halo components, and more centrally concentrated structures necessitate a smaller softening length (Athanassoula et al. 2000).

The tree code used in our simulations allows for an approximate interaction (as opposed to the direct summation force) between two tree nodes (cells or single bodies) only if their critical spheres do not overlap (Dehnen 2000a, 2002). The critical spheres are centred on the centre of mass of the nodes and have radii $r_{\rm crit} = r_{\rm max}/\theta$, where $r_{\rm max}$ is the radius containing all particles in the node and θ is the tolerance parameter (opening angle). In our simulations we use $\theta = 0.5$.

In order to have sufficiently small time-steps in the area around the CMC, we used adaptive time-stepping with the block-step scheme (time steps differ by factors of 2 and are hierarchically nested). In most simulations we used six levels, in such a way that the longest time-step is 2^{-6} and the shortest 2^{-11}. For the numerically more demanding simulations (with a CMC of very high mass or very small radius) we used seven levels and a smallest time-step of 2^{-12}. The time-step levels are adapted in an (almost) time-symmetric fashion to be on average

$$\tau = \min\{f_a/a,\, f_\Phi/|\Phi|\}, \tag{4}$$

where f_a and f_Φ are constants, a is the modulus of the acceleration, and Φ is the potential. We adopted $f_a = 0.01$ and $f_\Phi = 0.015$, thus ensuring that the smallest time-step bin contains of the order of a few per cent of the particles.

We model the disc with 200 000 and the halo with roughly 1000 000 particles. With these settings, the energy conservation after the CMC growth (during CMC growth energy is not conserved) was always better than one part in 1 000, and, in most cases, of the order of a couple of parts in 10 000.

2.3 The CMC

Following previous studies (NSH and SS), we model the CMC by a Plummer sphere of potential

$$\Phi_{\rm CMC}(r) = -\frac{GM(t)}{\sqrt{r^2 + r_{\rm CMC}^2}}, \tag{5}$$

where $M(t)$ is the mass of the CMC at time t, and $r_{\rm CMC}$ is its radius. In order to avoid transients, the CMC is introduced gradually with

$$\frac{M(t)}{M_{\rm CMC}} = \begin{cases} 0 & : \quad t \leqslant t_{\rm in} \\ \frac{3}{16}\xi^5 - \frac{5}{8}\xi^3 + \frac{15}{16}\xi + \frac{1}{2} & : \quad t_{\rm in} < t < t_{\rm grow} \\ 1 & : \quad t \geqslant t_{\rm grow} \end{cases} \tag{6}$$

where $\xi = 2\,(t - t_{\rm in})/(t_{\rm grow} - t_{\rm in})\;1$ and $t_{\rm in}$ is the time at which the CMC is introduced (Dehnen 2000b). Thus the mass, as well as its first and second derivatives are continuous functions of t. The radius $r_{\rm CMC}$ of the CMC is kept constant with time. In the following, since we are interested in the time evolution after the CMC is introduced, we measure time from the time when the CMC was introduced, i.e. from $t_{\rm in}$.

Some of the software used in the analysis has already been described in AM02, and we refer the reader to that paper for more information. Our runs are listed in Table 1. The first column gives

Table 1. Parameters for the CMC.

Simulations	Model type	$M_{\rm CMC}$	$r_{\rm CMC}$	$t_{\rm grow}$
MH	MH	0.	–	–
MH_1	MH	0.05	0.01	100
MH_2	MH	0.10	0.01	100
MH_3	MH	0.10	0.005	100
MH_4	MH	0.20	0.01	100
MH_5	MH	0.10	0.01	200
MD	MD	0.	–	–
MD_1	MD	0.05	0.01	100
MD_2	MD	0.10	0.01	100
MD_3	MD	0.10	0.005	100
MD_4	MD	0.20	0.01	100
MD_5	MD	0.10	0.01	200
MD_6	MD	0.04	0.01	100
MD_7	MD	0.03	0.01	100
MD_8	MD	0.02	0.01	100
MD_9	MD	0.01	0.01	100
MD_{10}	MD	0.1	0.1	100
MD_{11}	MD	0.1	0.08	100
MD_{12}	MD	0.1	0.05	100
MD_{13}	MD	0.1	0.02	100

[2] Streaming SIMD Extensions; SIMD = Single Instruction Multiple Data.

the name of the run and the second one the type of the model. The mass of the CMC, $M_{\rm CMC}$, its radius, $r_{\rm CMC}$, and its growth time, $t_{\rm grow}$, are given in the third, fourth and fifth columns, respectively.

3 EVOLUTION PRIOR TO THE INTRODUCTION OF THE CMC

The formation and evolution of the bar in *N*-body simulations have already been extensively described in the literature. Here we will only summarize very briefly some results from AM02, A02, and A03, which are necessary for discussing the simulations at hand, and will refer the interested reader to these papers for more information (see also Athanassoula 2005a).

Barred galaxies evolve by redistributing their angular momentum. This is emitted mainly by near-resonant material in the inner disc and absorbed by near-resonant material in the outer disc and in the halo. The amount of angular momentum that can be emitted and absorbed depends on the amount of near-resonant material and on how dynamically hot/cold this is. Since there is relatively little material in the outer disc, the halo can play a major role in this exchange, even though the material that constitutes it is relatively hot. Thus, bars immersed in massive haloes can grow stronger than bars immersed in weak haloes, and very much stronger than bars immersed in rigid haloes. Models in which the halo plays a substantial role in the dynamics within the inner four or five disc scalelengths, while being also sufficiently cool to absorb considerable amounts of angular momentum, were termed MH (for massive halo) in AM02. Such models form strong bars. Contrariwise, models in which the disc dominates the dynamics within that region form less strong bars and were termed MD (for massive disc) in AM02. Owing to the considerably different dynamics in the two cases, we decided to study the effect of a CMC in two models, one of MH-type and one of MD-type.

The observable properties of the bars that grow in these two types of models are quite different (see AM02 for a more complete discussion). MH-type bars are stronger (longer, thinner and more massive) than MD-type bars. Viewed face-on, they have a near-rectangular shape, while MD-type bars are more elliptical. Viewed side-on,[3] they show stronger peanut shapes and sometimes (particularly towards the end of the simulation) even 'X' shapes. Bars in MD-type models are, on the other hand, predominantly boxy when viewed side-on.

Fig. 1 shows the projected density radial profiles of the two types of bars seen face-on. The results are in good agreement with what was found by AM02 (see their fig. 5 and their section 5). The radial profile along the major axis of the MD bar decreases with radius without showing any clear change of slope at the end of the bar. For the MH type, however, the profile along the bar major axis is quite different. It has a relatively flat part in the bar region which is followed by a sharp drop at the end of the bar. These two different types of profiles have also been found in observations of barred galaxies. Elmegreen & Elmegreen (1985), using blue and near-infrared surface photometry of a sample of 15 barred galaxies, classified the photometric profiles in the bar region into two groups: the flat ones and the exponentially decreasing ones, i.e. the two types found in our two fiducial simulations. The importance of these two types of profiles for bar destruction will be discussed in the final section.

[3] The edge-on view, in which the bar is viewed perpendicularly to its major axis, is called side-on. The edge-on view, in which the bar is viewed along its major axis, is called end-on.

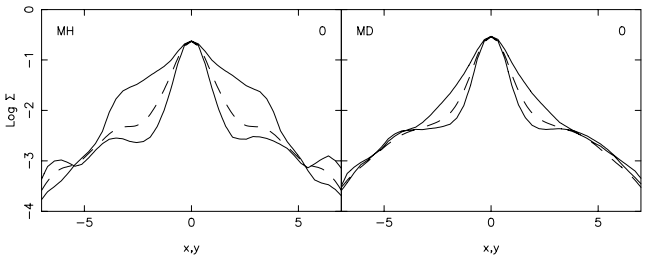

Figure 1. Projected density profiles along the bar major and minor axes (solid) and azimuthally averaged (dashed). The disc is seen face-on. The left-hand panel corresponds to model MH and the right-hand one to model MD, both at the time the CMC is introduced.

4 EVOLUTION AFTER INTRODUCTION OF THE CMC

4.1 The effect of the CMC

4.1.1 MH-type bars

The effect of a CMC on a MH-type bar is shown in the left-hand panels of Fig. 2. The upper left-hand panel shows the three views of the disc component before the CMC is introduced. The face-on view shows a strong bar with ansae at its ends, similar to what is seen in many early-type strongly barred galaxies (good examples can be seen on pages 42 and 43 of the Hubble Atlas, Sandage 1961). The side-on view shows a clear peanut, or mild 'X', shape, of extent somewhat shorter than the bar, as expected (for a discussion see Athanassoula 2005b). Seen end-on, the bar can easily be mistaken for a bulge and can only be distinguished from it by kinematical measurements (Bureau & Athanassoula 2005; Athanassoula 2005a,b).

The middle and lower panels on the left-hand side of Fig. 2 show the disc component at $\Delta T = 400$ after the CMC has been introduced. With the units proposed in Section 2.1, this is equivalent to 5.6 Gyr. The mass of the CMC in these two cases is 0.05 and 0.1, respectively, and $r_{\rm CMC} = 0.01$. We note that the smaller of the two masses did not destroy the bar, but made it considerably weaker. In particular, the final bar is considerably shorter. Since its width has not changed considerably, its axial ratio (minor to major axis) has become considerably larger. The heaviest of the two CMCs has not destroyed the bar either, although its mass is as much as 10 per cent of that of the disc. The resultant bar is, however, rather short and oval. A CMC with a mass of 0.2 is sufficiently massive to destroy the bar and make the disc near-axisymmetric (not shown here).

The CMC also changes the vertical structure of the bar. Before the introduction of the CMC, and seen side-on, the bar has a peanut shape, or mild 'X' form, with a maximum vertical extent at a distance from the centre roughly equal to three-quarters of the bar length and a minimum in between the two maxima. The middle left-hand panel, corresponding to $M_{\rm CMC} = 0.05$, shows that the bar seen side-on has a boxy shape, with a roughly constant vertical extent. The radial extent of this boxy feature is roughly the same as that of the peanut before the CMC was introduced. Thus, although the CMC brought a considerable decrease of the bar length seen face-on, it brought little, if any, decrease of the radial extent of the vertically extended feature. The more massive CMC, $M_{\rm CMC} = 0.1$, brings a stronger change to the vertical structure. Seen side-on, the shape is more elliptical than boxy. Therefore the introduction of a CMC changes the side-on outline from peanut to boxy, or, for very massive CMCs, to elliptical. The radial extent of these features, however, does not change much. The CMC also makes changes in the outline in the

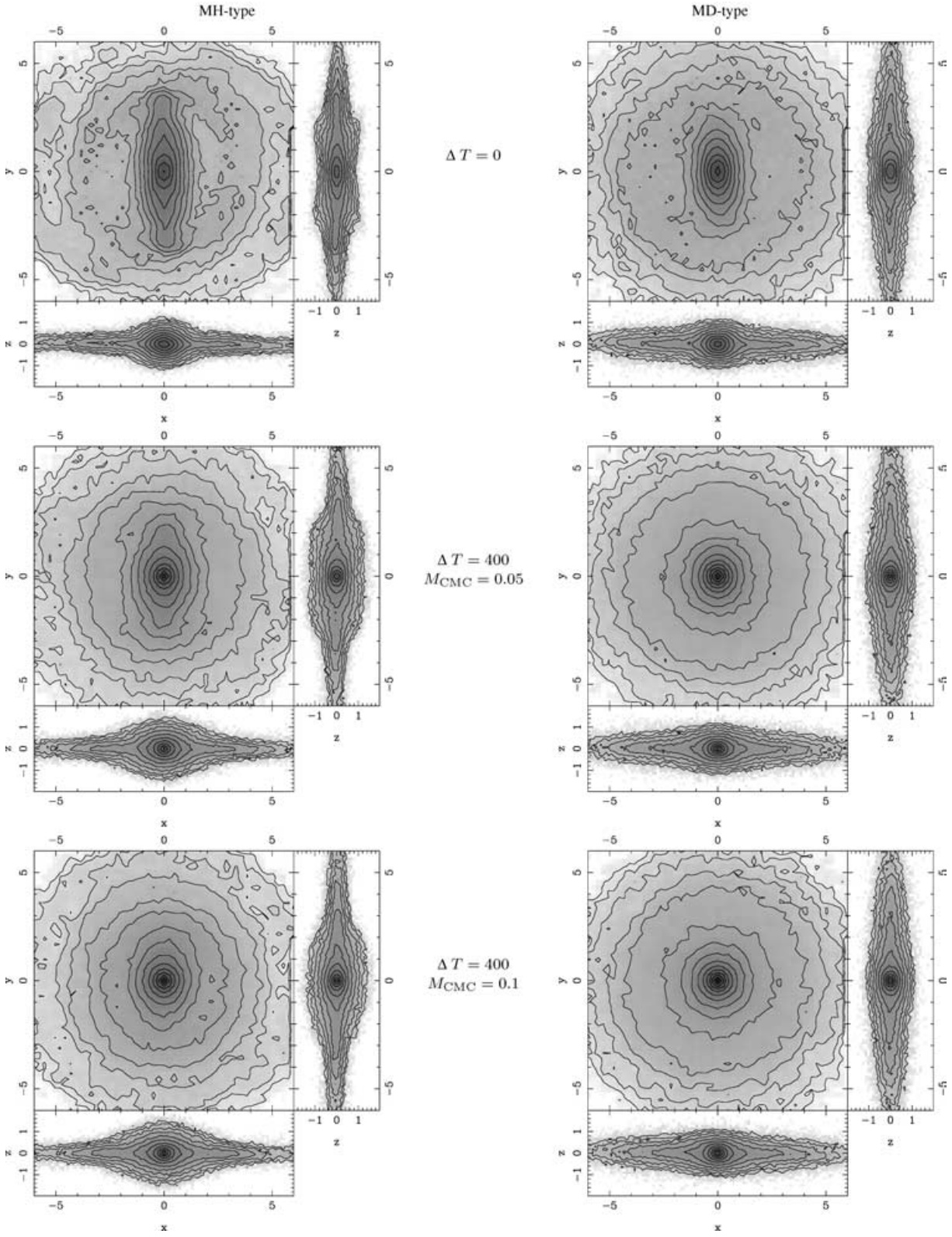

Figure 2. Effect of a CMC on a MH-type (left) and MD-type (right) model. The upper panels show the disc component at the time the CMC is introduced and the others at $\Delta T = 400$ later. The mass of the CMC is 0.05 for the middle two panels and 0.1 for the lower two, while $r_{\rm CMC} = 0.01$ in both cases. Each subpanel shows one of the three orthogonal views of the disc component. The right-hand subpanel gives the edge-on side-on view, the lower subpanel gives the edge-on end-on view, and the main subpanel the face-on view. The projected density of the disc is given by grey-scale and also by isocontours (spaced logarithmically).

end-on view. The vertical extent increases in the central region, and the bulge-like feature becomes considerably more extended radially.

4.1.2 MD-type bars

The right-hand panels of Fig. 2 are similar to the left-hand panels, but for an initially MD-type bar. Before the CMC is introduced the bar is both fatter and shorter, i.e. less strong than that of the previous example, in agreement with the results of AM02. It also has no ansae. Seen side-on, it has a boxy structure, but no peanut shape. The middle and lower right-hand panels show the disc component at $\Delta T = 400$ after the CMC has been introduced. The mass of the CMC in these two cases is again 0.05 and 0.1, respectively, and $r_{\rm CMC} = 0.01$. We note that the introduction of the CMC makes major changes. Seen face-on, the bar has nearly disappeared even for $M_{\rm CMC} = 0.05$, where only close scrutiny reveals that the isophotes are not circular, but slightly elongated, in what used to be the bar region. For $M_{\rm CMC} = 0.1$, there is no longer any trace of the bar, the isophotes being circular within the measuring errors. Seen side-on, the boxiness has more or less disappeared for $M_{\rm CMC} = 0.05$, and there is definitely no trace left by $M_{\rm CMC} = 0.1$. Thus, judging from the morphology of the three orthogonal views, the models with $M_{\rm CMC} = 0.1$ or 0.05 qualify as SA galaxies, i.e. galaxies with no bar. Thus, even a moderately light CMC can destroy the bar in MD-type models. This is contrary to what was found above for MH-type models, and constitutes an important difference between the two models.

To check whether a less massive CMC can still destroy the bar we ran four more simulations with $M_{\rm CMC}$ equal to 0.04, 0.03, 0.02 and 0.01, respectively. In all four cases the bar is clearly visible by the end of the simulation, although considerably weakened. We also ran simulations with $M_{\rm CMC} = 0.1$ and $r_{\rm CMC} > 0.01$ to check whether the bar is destroyed even for CMCs with such large radii. We found that $r_{\rm CMC}$ has to be at least as large as 0.1 for the bar not to be destroyed.

4.2 The bar strength

4.2.1 The bar strength as a function of time and radius

Fig. 3 gives, for six simulations, the amplitude of the $m = 2$ (bisymmetric) component of the mass/density distribution as a function of both time and radius. This is a simple measure of the bar strength. The results for higher m values will be discussed in the next subsection. The left-hand panels correspond to two reference simulations in which no CMC has been introduced. They show clearly a secular evolution, during which the bar becomes slowly and steadily stronger. We note that the maximum amplitude increases, but also that both the innermost and the outermost parts become gradually more bisymmetric.

The picture is different for simulations with a CMC. At early times, up to 20 or 30 time units after the CMC has been introduced, the evolution continues more or less as if no CMC had been introduced. This is presumably because the CMC has to reach a limiting mass before its effect can be felt by the bar and/or because the orbits in the bar region take some time to adjust. This time interval is longer in the case of less massive CMCs. After that a second time interval starts, which lasts roughly until the time the CMC reaches its maximum mass. During this second phase the amplitude drops abruptly with time. A third time interval starts after that and lasts until the end of the simulation. Unless the bar has totally disappeared after the end of the second interval, its amplitude continues to decrease in this third phase, but at a considerably slower rate than in the second

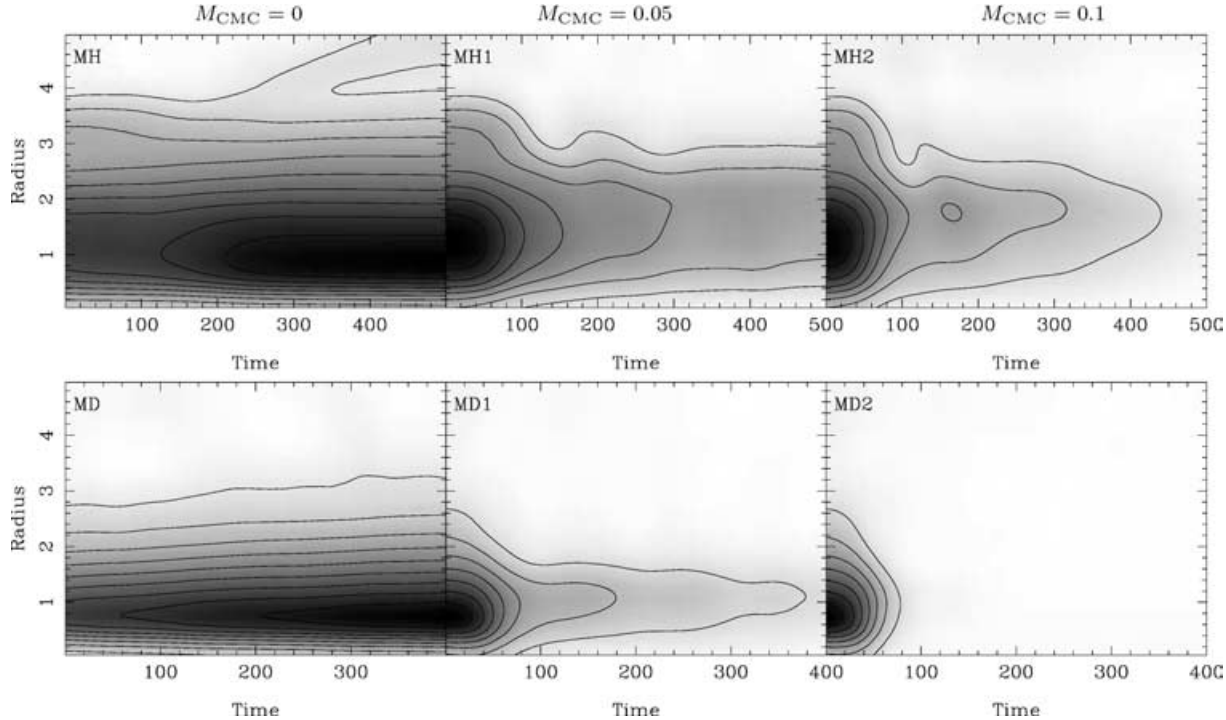

Figure 3. Bar amplitude ($m = 2$ Fourier component of the amplitude) as a function of time and radius, for the three MH-type (top) and the three MD-type (bottom) simulation, from which snapshots are shown in the left- and right-hand panels of Fig. 2, respectively. The grey-scale and isocontour levels are set separately in each panel, so as to highlight the relevant features. The isocontour levels are spaced linearly and darker shades correspond to higher amplitudes. The name of the simulation is given in the left-hand corner of each panel.

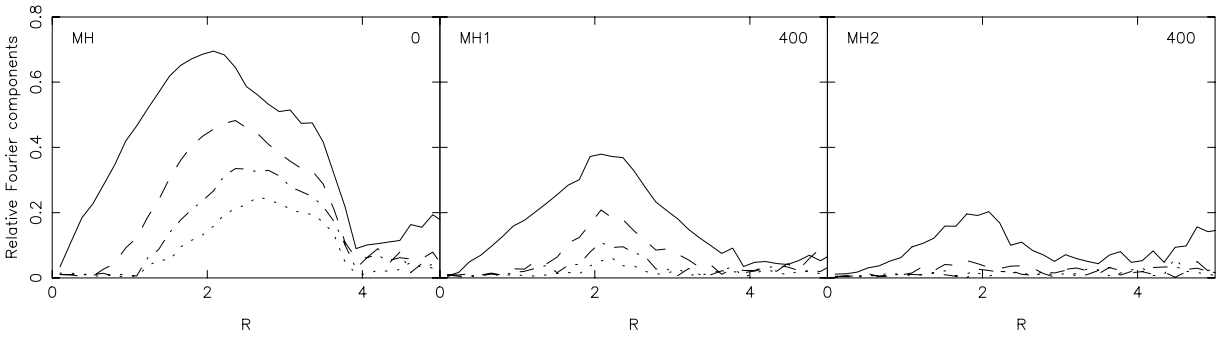

Figure 4. Ratio of amplitudes of the $m = 2$ (solid), 4 (dashed), 6 (dot–dashed) and 8 (dotted) Fourier components of the density with the $m = 0$ component. The name of the simulation is given in the upper left-hand corner and the time since the introduction of the CMC in the upper right-hand corner of each panel.

one. The distinction between the second and the third time intervals is sharper for MD-type than for MH-type models, and for more massive CMCs. Fig. 3 shows clearly that the maximum amplitude decreases steadily with time, but also that both the innermost and the outermost parts of the disc become gradually more axisymmetric. This is in agreement with what is seen in Fig. 2. Indeed, it is clear there that at $\Delta T = 400$ after the CMC was introduced the bar has become shorter and the innermost isophotes have become rounder. The corresponding time evolution can be followed in Fig. 3.

Comparison of the upper and lower panels of Fig. 3 shows that a given CMC can destroy MD-type bars more efficiently than it can MH-type ones. Moreover, comparison of the central and right-hand columns of panels shows that more massive CMCs are more efficient for bar destruction, as expected.

4.2.2 Higher m values

Fig. 4 shows the relative amplitude of the $m = 2, 4, 6$ and 8 Fourier components of the density for simulations of MH-type bars. They have been calculated as described in AM02. Before the introduction of the CMC (left-hand panel) all components have high amplitudes. Specifically, their maxima are 0.7, 0.48, 0.33 and 0.25, for $m =$ 2, 4, 6 and 8, respectively. The introduction of the CMC brings a considerable decrease of all of these values. Thus, for $M_{\rm CMC} = 0.05$ and $\Delta T = 400$ the maxima of the amplitudes for the various ms fall to 0.54 ($m = 2$), 0.43 ($m = 4$), 0.32 ($m = 6$) and 0.25 ($m = 8$) of the initial maximum values. For $M_{\rm CMC} = 0.1$ and the same time lapse, the $m = 2$ amplitude falls to 0.3 of its initial value, while the other components drop to the noise level.

Fig. 4 quantifies the effect of the CMC and, more importantly, shows that it has a stronger effect on the higher m components. The latter can be understood as follows. As can be seen from the left-hand panel of Fig. 4, before the CMC is introduced the radius at which the relative amplitude has its maximum increases with m and comes closer to the outer regions of the bar. These regions, as we saw in Sections 4.1 and 4.2.1, are affected first and tend to axisymmetry faster. In this way, the higher m components will be affected before the lower ones. This argument is further re-enforced when we look at the positions of the maxima. For $m = 2$ the maximum is at roughly 2.1 and stays there after the CMC has been introduced, as can be seen by comparing the left-hand panel with the middle and right-hand ones. The maximum of the $m = 4$ and 6 components is roughly at 2.4 at the time the CMC is introduced, however, and moves to 2.1, i.e. the same radius as that of the $m = 2$ maximum, 400 time units after a CMC with $M_{\rm CMC} = 0.05$ is introduced. Since the higher m components are affected less than the lower m ones, the isodensity contours become fatter and/or less rectangular (and thus more elliptical). Fig. 2 confirms this.

Fig. 5 gives similar information, but for MD-type simulations. As already discussed in AM02, MD-type models have lower values of all the amplitudes and also lower values of the relative amplitude of the higher m components than MH-type models. Thus, for MD-types, the CMC destroys the higher m components even for relatively small values of the CMC mass. This is illustrated in Fig. 5, where we show results for two models with $M_{\rm CMC}$ equal to 0.01 and 0.02, respectively.

4.3 Velocity dispersion along the bar major axis

Fig. 6 shows the three components of the velocity dispersion as a function of distance from the centre. They have been calculated as described in AM02. That is, we isolate a thin strip of particles centred

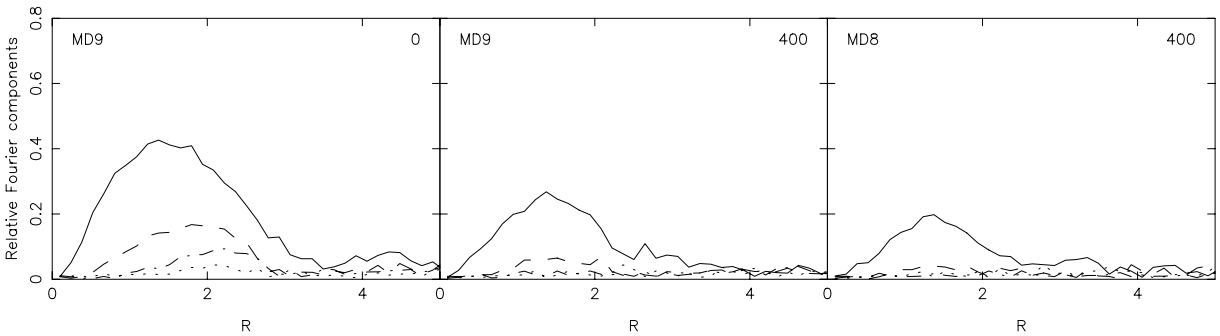

Figure 5. As Fig. 4, but for MD-type models.

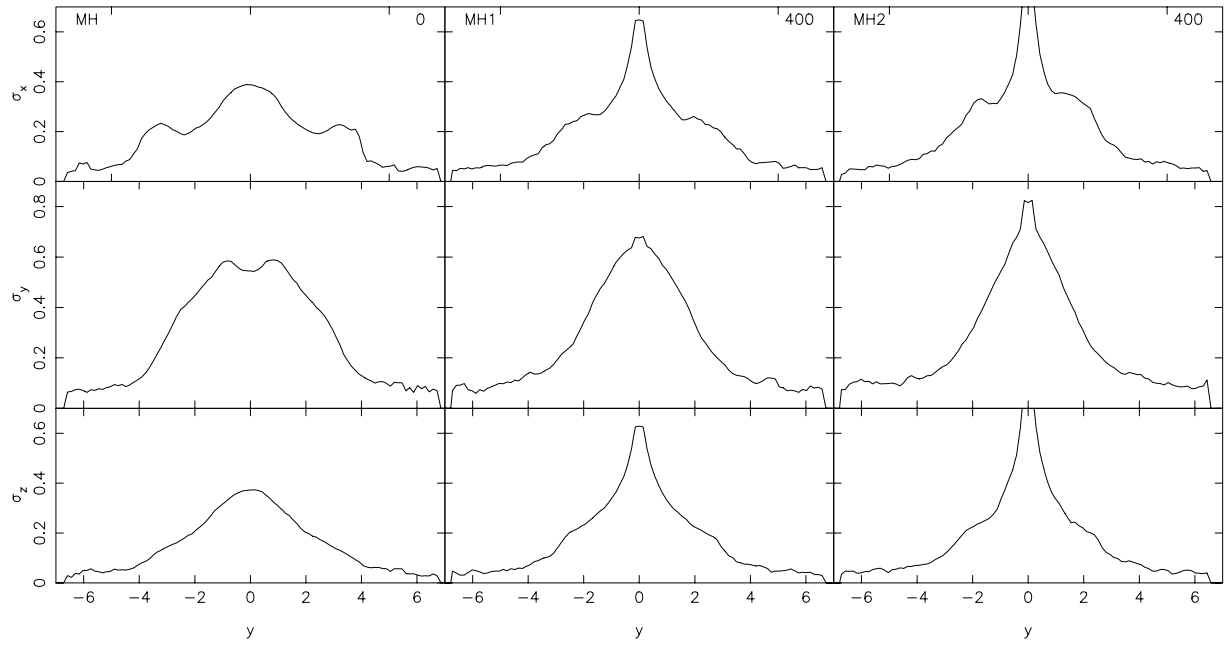

Figure 6. Velocity dispersion as a function of distance from the centre, as discussed in Section 4.3. The left-hand column of panels corresponds to MH simulations at the time the CMC is introduced, while the central and right-hand columns of panels correspond to simulations MH_1 and MH_2, respectively. The three components of the velocity dispersion, σ_x, σ_y and σ_z, are given in the upper, middle and lower rows of panels, respectively. The name of the simulation is given in the upper left-hand corner and the time since the introduction of the CMC in the upper right-hand corner of the upper panels.

on the bar major axis and having a width of 0.07. The distance from the centre is calculated along this strip. In this way, we avoid making an integration along the line of sight, since this would impose the choice of a particular viewing angle. We also bring out more clearly the information on the motions of particles near the bar major axis, which is of particular use when comparing with periodic orbit structure. Nevertheless, any comparison with observations can only be rough, since our presentation gives information only on a subset of the orbits.

At the time the CMC is introduced, the velocity dispersions of model MH show features characteristic of MH-type models (see AM02 for a more complete description). The σ_x component (perpendicular to the bar major axis) has a clear maximum at the centre and two secondary maxima on either side of it. These could be the result of orbits trapped around x_1 periodic orbits with loops at their apocentres, and/or the result of the superposition of orbits trapped around elliptical and around rectangular shaped periodic orbits. The CMC turns these maxima into plateaus and moves them nearer to the centre. Both effects could be expected. Indeed, these maxima are only found for strong bars (AM02), while the CMC has reduced the bar strength. Furthermore, these structures are linked to the end of the bar, which is shortened by the effect of the CMC, see Sections 4.1 and 4.2.1. Of course the clearest effect of the CMC is to raise very substantially the central velocity dispersion, and more strongly so for the most massive CMCs.

At the time the CMC is introduced, the σ_y component has a small, but characteristic, minimum at the centre, surrounded closely by two maxima on either side. Since the σ_y is the component parallel to the bar major axis, this feature should be mainly seen in edge-on barred galaxies that are viewed nearer to end-on than to side-on. The CMC obliterates this feature and creates, instead, a clear central maximum, as for σ_x. The σ_x and σ_y components have quite different values at the centre in the case with no CMC. As expected, however, the velocity distribution in the central regions becomes more isotropic in the cases with a CMC, and more strongly so for the most massive CMCs.

The MD-type models show no clear characteristic features on their velocity dispersion profiles (see fig. 13 of AM02). Thus the CMC only introduces a sharp maximum at the centre, clear in all three components of the velocity dispersion, as seen already in the MH-type models.

4.4 CMC radius and growth time

We ran two simulations with smaller values of $r_{\rm CMC}$ (see Table 1) and found that more centrally concentrated CMCs are more efficient for bar destruction, thus confirming a result already found by Hasan et al. (1993), with orbital calculations, and by SS, with simulations.

We also ran two simulations with a larger value of $t_{\rm grow}$ (see Table 1) and confirmed a result already found by SS and by HH, namely that the value of $t_{\rm grow}$ does not have much influence on the final bar weakening. It only influences the duration of the initial strong decrease. The transition between the initial strong decrease and the later milder one is sharper in simulations with larger $M_{\rm CMC}$ and/or smaller $r_{\rm CMC}$ (see bottom panels in Fig. 7).

4.5 Pattern speed

NSH stated that the introduction of the CMC results in an increase of the bar pattern speed. In order to assess further the effect of the CMC on the bar pattern speed, we measured this quantity in our simulations. This was not always easy, since in many cases the bar amplitude is so weak that the measurement was either not possible or gave a very uncertain value. In most cases, some smoothing was necessary. Nevertheless, from the cases in which the measurement is sufficiently precise, we can clearly see that the pattern speed *increases* with time, as the bar becomes weaker. This is shown for two sets of MD-type simulations in Fig. 7, and for MH-type simulations

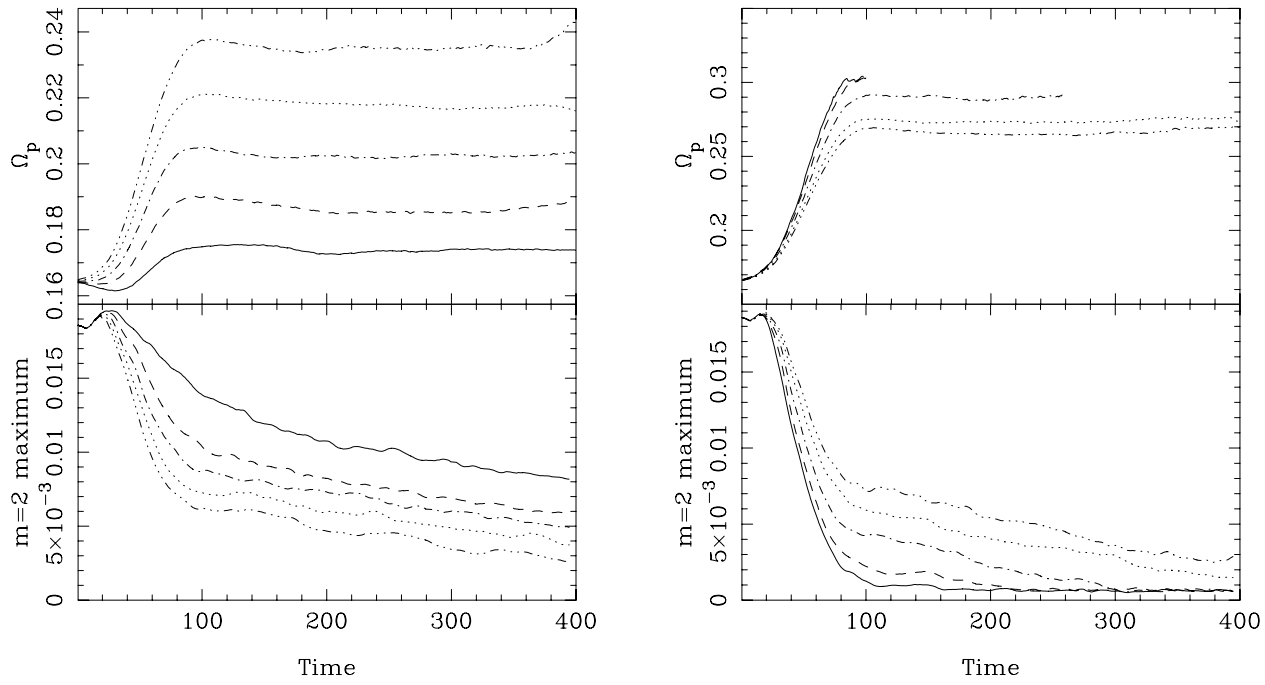

Figure 7. The upper panels give the pattern speed of the bar as a function of time. For some simulations and times the bar is not sufficiently strong to allow a correct measurement of the pattern speed, so we give no estimates. The lower panels give, for comparison, a measure of the bar strength, also as a function of time. As such a measure we use the maximum value of the amplitude of the $m = 2$ component of the mass. The left-hand panels refer to a series of simulations with different $M_{\rm CMC}$: $\rm MD_9$ (solid), $\rm MD_8$ (dotted), $\rm MD_7$ (dot–dashed), $\rm MD_6$ (dashed) and $\rm MD_1$ (treble-dot–dashed). The right-hand panels correspond to a series of simulations with different $r_{\rm CMC}$: $\rm MD_2$ (solid), $\rm MD_{13}$ (dotted), $\rm MD_{12}$ (dot–dashed), $\rm MD_{11}$ (dashed) and $\rm MD_{10}$ (treble-dot–dashed).

in Fig. 8. For comparison, we also plot a measure of the bar strength as a function of time. As such we have chosen the maximum value of the amplitude of the $m = 2$ component of the mass. Results found with other measures of the bar strength are similar.

The left-hand panels of Fig. 7 give results from a series of simulations with different values of the mass of the CMC, namely simulations $\rm MD_9$ ($M_{\rm CMC} = 0.01$), $\rm MD_8$ (0.02), $\rm MD_7$ (0.03), $\rm MD_6$ (0.04) and $\rm MD_1$ (0.05). In the very first 20 time units or so, the bar strength increases, as in simulations with no CMC. During this time, at least in simulations with small CMCs, the pattern speed decreases, again as in simulations with no CMC. This is presumably a result of the fact that the CMC has not grown enough to influence the evolution sufficiently to reverse the trend. This reversal indeed occurs at later times. We note that the bar speed increases noticeably up to time 100, while the CMC mass increases and the bar strength decreases most strongly. At later times there may still be an increase in the pattern speed, but it is very small and the data are too noisy to assess it with any certainty.

The right-hand panels of Fig. 7 give similar results, but now from a series of simulations with different values of the radius of the CMC, namely simulations $\rm MD_2$ ($r_{\rm CMC} = 0.01$), $\rm MD_{13}$ (0.02), $\rm MD_{12}$ (0.05), $\rm MD_{11}$ (0,08) and $\rm MD_{10}$ (0.1). For the value of $M_{\rm CMC}$ used in this sequence ($M_{\rm CMC} = 0.01$) and the smallest of our $r_{\rm CMC}$, the bar is practically destroyed by the time the mass of the CMC has reached its final value. Thus CMCs with a yet smaller radius give the same result. The very short-lived initial increase of the bar strength is less clear here than in the previous set of simulations. The basic result, however, stays the same.

Fig. 8 shows similar plots, but now for MH-type simulations. The results are similar; that is, there is an increase in the pattern speed during the time the strength of the bar decreases sharply. This increase is quite noticeable in cases in which the decrease of the

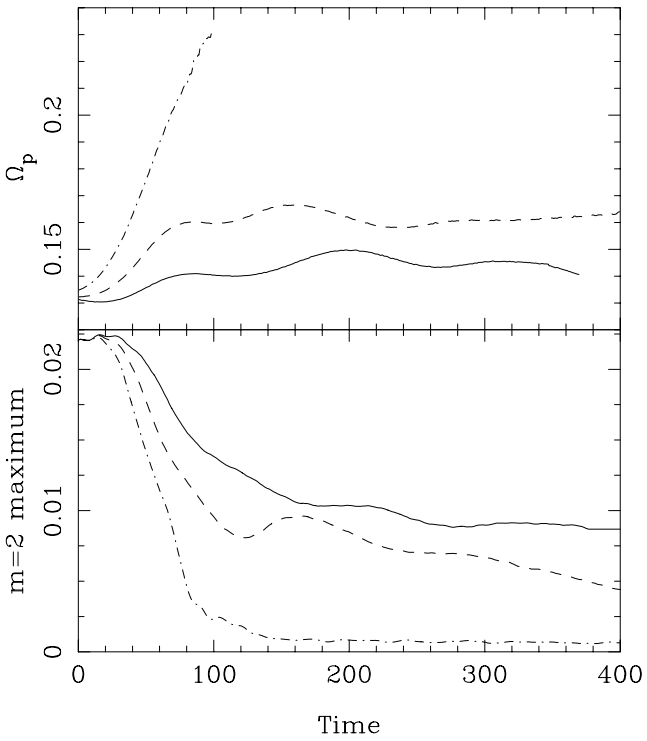

Figure 8. As for Fig. 7, but for MH-type models. Results are given for three simulations with different $M_{\rm CMC}$: $\rm MH_1$ (solid line), $\rm MH_2$ (dashed) and $\rm MH_3$ (dot–dashed).

bar strength is important, and considerably less so in cases with a milder decrease of the bar strength (as MD_9 or MH_1).

5 SUMMARY AND DISCUSSION

5.1 Bar survival and destruction

In this paper we have studied the effect of a central mass concentration (CMC) on the bar that harbours it. We find that the CMC leads to a decrease of the bar strength, which in some cases can be sufficiently important to lead to bar destruction. More massive and/or more concentrated CMCs are more efficient. The effect of the CMC depends also on the type of bar model. Strong bars, which we call MH-type because they form in simulations with massive haloes, and which are morphologically similar to Elmegreen & Elmegreen's (1985) flat-profile bars, are less prone to destruction than weaker bars, which we call MD-type because they form in simulations with massive discs, and which are morphologically similar to Elmegreen & Elmegreen's exponential-profile bars.

The effect of the CMC is strongest in the innermost and the outermost parts of the bar, where it makes the density distribution more axisymmetric. This leads to shorter and fatter bars, whose isodensity contours are more elliptical than rectangular. The CMC also affects the pattern speed of the bar, which grows noticeably while the mass of the CMC grows and the strength of the bar decreases strongly. This is in good agreement with the anticorrelation between bar strength and pattern speed found in A03 (see figs 16 and 17 in that paper). The CMC also influences the velocity dispersions. In particular, after the introduction of the CMC, the velocity dispersion profiles along the bar major axis show a strong central maximum, while the secondary maxima on either side of the centre, seen in the side-on projection of strong bars, become weaker and approach the centre.

In order to understand why a given CMC can destroy a bar in some cases, while only weakening it in others, it is necessary to study the time evolution of the orbital structure in the two cases. For this, it is necessary to study the orbital structure at a sequence of times during the evolution by calculating the potential and pattern speed at these times and using the corresponding positions and velocities of the simulation particles (as done in, for example, A02 and A03). The evolution of the orbital structure along this time sequence will give information on the evolution of the orbital structure during the simulation and should help to explain the difference between the effects of a CMC on MH-type and on MD-type bars. This analysis is beyond the scope of this paper and will be the subject of a future paper. It is possible, however, to make some remarks at this stage. A MH-type bar that survived with a decrease of its amplitude was initially thinner, i.e. had a smaller ratio of minor to major axis, than a MD-type bar that was destroyed. This means that the orbits in the former are more eccentric than those in the latter (Athanassoula 1992a); that is, for a given orbital major axis, the particles in the former will come nearer to the CMC than in the latter. Thus, one would expect that the bar structure in the MH-type bar would be affected more than the bar structure in the MD-type bar, and this is indeed what is found by Hasan & Norman (1990) in their orbital calculations. Furthermore, as can be seen in Fig. 1, the density distribution in MH-type bars is more centrally concentrated than in MD-type bars, so that the particles come closer to the CMC. Both effects suggest that MH-type bars could be destroyed more easily, and yet fully self-consistent simulations show the opposite.

It is not entirely clear what is wrong with this naive reasoning. Possibly, the orbital structure of planar bars, as studied by Hasan & Norman and HH, is a bad representation of the orbits actually populated, which extend to non-negligible heights. Indeed, Skokos, Patsis & Athanassoula (2002) have shown that the backbone of the bar is formed by the 3D families of the x_1 tree, and not by the 2D x_1 family. Thus, the fact that the planar orbits are unstable does not necessarily imply that the bar has to be destroyed. Finally, the 3D orbital-structure study of Hasan et al. (1993) is restricted to a single bar model and thus cannot shed any light on the differences between MH-type and MD-type bars.

In addition, the halo may play a role. Indeed, in galaxies with no CMC, MH-type haloes can absorb much more angular momentum from the bar than MD-type haloes, thus causing the bar to grow stronger in MH-type galaxies (A03). A similar effect could also occur in disc galaxies with a CMC. In other words, in galaxies with a CMC, the extra angular momentum that can be absorbed by the MH-type haloes could well cause the bar to decay less in MH-type than in MD-type galaxies, which is indeed what our simulations show. This alternative could also explain why SS find only mild differences between their strong and their weak bars. Indeed, if the difference arises from the halo, it would not show in these simulations, which have a rigid halo.

5.2 Comparison with previous work

There is good qualitative agreement between the results of all N-body studies so far, namely NSH (Norman et al. 1996), SS (Shen & Sellwood 2004), HH (Hozumi & Hernquist 2005), and our study. First and foremost, all find that the growing CMC results in a decrease of the bar strength. The disagreement is more quantitative than qualitative, and concerns whether the decrease in bar amplitude is sufficiently strong to destroy the bar. There are further agreements, in that the pattern speed increases as the bar strength decreases (NSH and this study), and that more massive and/or more centrally concentrated CMCs weaken the bar more than less concentrated ones (all studies). All the above are also in agreement with orbital-structure studies (Hasan & Norman 1990; Hasan et al. 1993). Finally, there is agreement that $t_{\rm grow}$ does not have much of an influence on the final bar weakening, but only influences the rate at which the bar strength decreases.

Quantitative comparisons are much more difficult to make, mainly because of the differences between the various studies. These differences include (1) the bar models, (2) the halo models (live or rigid), (3) the Poisson solvers and time-steps, (4) the dimensionality of the motion (2D or 3D), and (5) the initial conditions.

5.2.1 Norman et al. (1996) and Shen & Sellwood (2004)

Despite all these differences, NSH, SS and our study all agree that a CMC mass of at least a few per cent of the disc mass is required to destroy a bar. SS find that a CMC with $M_{\rm CMC} = 0.04$ and $r_{\rm CMC} = 0.001$ is necessary to destroy the bar, while for $M_{\rm CMC} = 0.1$ and $r_{\rm CMC} = 0.1$ the bar is weakened but not destroyed. Our fiducial $r_{\rm CMC}$ is between these values, and for $M_{\rm CMC} = 0.05$ or 0.1, the bar is destroyed in one of our bar models, and is considerably weakened in the other.

The most notable difference between these previous studies and ours is the treatment of the halo, namely rigid versus fully self-consistent, since SS used a rigid halo for computational economy. In support of the adequacy of this choice they run one simulation with a live halo and compare it with a rigid-halo case. Unfortunately, the two runs are not very similar initially, so an assessment of the importance of the halo response does not follow straightforwardly from a comparison. Indeed, fig. 8 in SS shows a difference in the

initial bar amplitude of the same order as the difference between their strong and weak bar cases (their fig. 5). Moreover, their comparison is done for a halo whose density is low in the disc region, which will certainly restrict the influence of the halo on the bar evolution. Simulations with a dense halo would necessarily show a much stronger influence. In particular, a rigid halo will not allow halo material to form a cusp around the CMC. Furthermore, the importance of a live halo for the correct description of bar evolution has been clearly demonstrated in some cases by comparing rigid- and live-halo simulations (A02). For these reasons, we have adopted a live halo in our simulations, and believe this to be crucial for a correct astrophysical understanding.

SS studied two bars of different strengths and found only mild differences. We, on the other hand, find significant differences between our MD-type and MH-type bars: the former is destroyed for $M_{\rm CMC} = 0.1$ and $r_{\rm CMC} = 0.01$, while the latter is only weakened. This is not a real disagreement, since the difference between the weak and strong bars of SS is considerably less than the difference between our MH-type and MD-type bars. However, if the robustness of our MH-type bars originates (at least partially) from the interaction with its halo, simulations like those of SS may not be suitable for interpreting the evolution of galaxies with massive haloes.

There are notable differences between the two sets of studies with respect to their softening. We use a softening of 0.03 (i.e. 0.02 Plummer equivalent), a fiducial $r_{\rm CMC}$ of 0.01, and a range of $r_{\rm CMC}$ values between 0.005 and 0.1. Thus our fiducial $r_{\rm CMC}$ is half the softening, while in most of our adopted range it is equal to or bigger than the softening. We also use a softening kernel that decreases faster than the standard Plummer one, thus limiting its effect at larger radii. To test further the effect of the softening, we ran a series of simulations with larger values of softening, namely 0.06 and 0.09 (i.e. equivalent Plummer softenings of 0.04 and 0.06), and found only very small differences, for example in the bar strength. This argues strongly that our softening is adequate for the problem at hand. SS have been bolder than us in the use of the softening. They use a softening of 0.02 for their strong-bar case, and 0.05 for their weak-bar case, while studying the effect of CMCs with $r_{\rm CMC}$ ranging between 0.0003 and 0.1, with a fiducial value of 0.001. This makes their softening 20 to 50 times larger than their fiducial $r_{\rm CMC}$, the ratio reaching, for their most concentrated CMC, roughly 67 for their strong-bar case and 167 for their weak-bar case. In their fig. 7, they compare three simulations with softenings of 3, 7 and 17 times the CMC radius, respectively, and find differences in the bar strength only of the order of, or smaller than, 10 per cent.

5.2.2 Hozumi & Hernquist (2005)

The recent study by HH differs notably from both previous studies (NSH and SS) and from ours. In particular, HH find that a CMC with 1 per cent or even 0.5 per cent of the disc mass is sufficient to destroy a bar (for $r_{\rm CMC} = 0.01$ disc scalelengths). It is not clear at this stage what actually causes this discrepancy. HH blamed the different initial conditions, in particular the fact that they have an exponential disc, while NSH and SS use a Kuzmin–Toomre disc. Our discs, however, are also initially exponential and yet our results are in agreement with those of SS, but not with those of HH. We discuss below some other possible explanations of the discrepancy.

One possibility is that there is a subtle numerical difference between the two sets of simulations, in particular in the resolution of their code and the time-stepping. A poor resolution, corresponding to large effective softening, should, however, decrease the mass of any cusp forming around the CMC and hence reduce the destructive effect. Furthermore, HH have tested the number of terms that they use and found it to be sufficient. An insufficiently small time-step may entail an artificial bar destruction. Both SS and this study use a variable time-step, which is very small in the vicinity of the CMC, contrary to HH, who use a constant time-step. In the same units as we use here, HH have $\Delta t = 0.01$, or 0.005, depending on the model. This contrasts with the time-step that we have adopted, which, in the vicinity of the CMC, is roughly 0.0005 or 0.0002. The time-steps can be compared with the dynamical time at $r \rightarrow 0$ due to the CMC alone:

$$t_{\rm dyn,\,CMC} = 2\pi\sqrt{r_{\rm CMC}^3/GM_{\rm CMC}} \qquad (7)$$

for a Plummer model (used by NSH, SS, and us) and $\sqrt{3/4}$ shorter for the CMC model of HH. For the $M_{\rm CMC} = 0.005$ model of HH, we find $t_{\rm dyn,\,CMC} \approx 0.077$.

An obvious difference between HH on the one hand and SS and our work on the other is that the former simulations are 2D, while the latter are 3D. Norman et al. (1996), however, compared 2D and 3D simulations and found no important differences capable of accounting for the discrepancy we wish to explain. Given that Norman et al. consider only a single bar model, it would be desirable to examine more models in order to understand better the relation between 2D and 3D results.

5.2.3 Simulations with gas

Gas flowing in a barred galaxy potential will form shocks along the leading edges of the bar (Athanassoula 1992b), leading to an important inflow that can create a CMC. A number of N-body+SPH calculations have followed this evolution and found that the CMC that is thus formed can destroy the bar (Friedli & Benz 1993; Friedli 1994; Berentzen et al. 1998). Friedli found that, when the gas is sufficiently concentrated so as to form a CMC of 2 per cent of the disc mass, the bar is destroyed in about 1 Gyr. Berentzen et al. found a very similar result when the CMC formed by the inflow had a mass equal to 1.6 per cent of that of the galaxy within 10 kpc and a characteristic radius of the order of a few hundred parsecs. The bar is destroyed also in the simulations of Bournaud & Combes (2002). The two first studies use SPH (Monaghan 1992) to model the gas, while the third one uses a sticky particle algorithm (Schwarz 1981).

The CMC mass and radius estimates obtained from such simulations cannot be compared with those obtained by purely N-body simulations. Of course, in both cases the growth of the CMC makes a large fraction of the x_1 orbits unstable, and this family is known to be the backbone of the bar (Contopoulos & Papayannopoulos 1980; Athanassoula et al. 1983). In cases including gas, however, there is an extra effect, absent from the purely stellar cases. It is now known that the growth of the bar is governed by the angular momentum exchanged between the inner parts of the disc (bar) and the halo plus outer disc (A03). In cases with gas, there is an extra component taking part in this exchange process. Berentzen et al. (2004) have shown that the gas, by giving angular momentum to the inner disc, will damp the bar growth. Thus the presence of a gaseous component should favour bar destruction so that the CMC mass necessary to achieve this should be smaller in cases with a sizeable gaseous component than in purely stellar cases.

5.3 Comparison with observations

As noted in the Introduction, the mass of observed supermassive black holes is of the order of 10^{-3} times the mass of the bulge that harbours them. Unfortunately, neither our simulations, nor those

of NSH, SS and HH, include any case with a live bulge. Bulges, however, are in general less massive than their corresponding discs, so the value of $10^{-3}M_{\rm d}$ can be considered as an upper limit of the supermassive black hole mass. This is two orders of magnitude lower than our fiducial value and one order of magnitude smaller than the smallest value considered here. Making comparisons with the CMC radius is less straightforward. Following previous studies, we assume that our results are relevant to supermassive black holes since the CMC radius is much smaller than its influence radius – more than an order of magnitude for our fiducial cases. Therefore, in as far as our results can be applied to supermassive black holes, they argue that these cannot destroy the bar that harbours them.

Observations show that important mass concentrations, sometimes as large as $10^9\,{\rm M}_\odot$, can often be found in the central parts of strongly barred galaxies (Sakamoto et al. 1999; Regan et al. 2001; Helfer et al. 2003; Kormendy & Kennicutt 2004; Jogee, Scoville & Kenney 2005). These are either in the form of molecular gas discs, or of discy bulges (for a description see Athanassoula 2005b). Simulations that do not include gas give only partial information on the effect of such a CMC on the bar, since they cannot evaluate the role of the gas in the angular momentum exchange. In other words, they can give information on the effect of the CMC as such, but not on the effect of its formation. The following discussion will therefore, by necessity, neglect the latter effect. Assuming a characteristic disc mass of $5 \times 10^{10}\,{\rm M}_\odot$, we obtain a ratio $M_{\rm CMC}/M_{\rm d} = 0.02$, i.e. five times smaller than our fiducial $M_{\rm CMC}$. The sizes of these CMCs are between 0.1 and 2 kpc, i.e. between 0.03 and 0.6 times the exponential disc scalelength of the Milky Way. Assuming that the characteristic scalelength is half the extent, we find that the corresponding values for $r_{\rm CMC}$, in the units used here, are between 0.015 and 0.3. Since in this paper we have used values of $r_{\rm CMC}$ between 0.005 and 0.02, the observed gaseous CMC will, for a given mass, be less destructive than the CMCs used here. We thus come to the conclusion that such CMCs, given their masses and notwithstanding the effect of their formation, are not capable of destroying bars.

Sakamoto et al. (1999) and Sheth et al. (2005) show that the degree of gas concentration in the central kiloparsec is higher in barred than in unbarred galaxies. This would not be possible if the molecular gas CMCs could destroy a bar. It is, however, in good agreement with our results. The torques from a bar can push gas to the centre, and, for a given gas reservoir, the stronger the bar the more important this central gaseous concentration will be (Athanassoula 1992b). It is thus reasonable to expect that, if the CMC does not destroy the bar, stronger gas concentrations will be found in barred than in unbarred galaxies, as is indeed borne out by the observations of Sakamoto et al. and Sheth et al.

ACKNOWLEDGMENTS

We thank A. Bosma and S. Hozumi for stimulating discussions and an anonymous referee for comments that improved the presentation. EA and JCL thank the INSU/CNRS, the region PACA and the University of Aix-Marseille I for funds to develop the computing facilities used for the calculations in this paper.

REFERENCES

Athanassoula E., 1992a, MNRAS, 259, 328
Athanassoula E., 1992b, MNRAS, 259, 345
Athanassoula E., 2002, ApJ, 569, L83 (A02)
Athanassoula E., 2003, MNRAS, 341, 1179 (A03)
Athanassoula E., 2005a, Cel. Mech. & Dyn. Astr., 91, 9
Athanassoula E., 2005b, MNRAS, 358, 1477
Athanassoula E., Misiriotis A., 2002, MNRAS, 330, 35 (AM02)
Athanassoula E., Bienayme O., Martinet L., Pfenniger D., 1983, A&A, 127, 349
Athanassoula E., Fady E., Lambert J. C., Bosma A., 2000, MNRAS, 314, 475
Athanassoula E., Dehnen W., Lambert J. C., 2003, in Engvold O., ed., Proc. IAU Highlights of Astronomy, Vol. 13. Astron. Soc. Pac., San Francisco, p. 355
Bahcall J. N., Wolf R. A., 1976, ApJ, 209, 214
Barnes J., Hut P., 1986, Nat, 324, 446
Berentzen I., Heller C. H., Shlosman I., Fricke K. J., 1998, MNRAS, 300, 49
Berentzen I., Athanassoula E., Heller C. H., Fricke K. J., 2004, MNRAS, 347, 220
Bournaud F., Combes F., 2002, A&A, 392, 83
Bureau M., Athanassoula E., 2005, ApJ, 626, 159
Contopoulos G., Papayannopoulos T., 1980, A&A, 92, 33
Dehnen W., 2000a, ApJ, 536, L39
Dehnen W., 2000b, AJ, 119, 800
Dehnen W., 2001, MNRAS, 324, 273
Dehnen W., 2002, J. Comp. Phys., 179, 27
Dehnen W., Odenkirchen M., Grebel E. K., Rix H.-W., 2004, AJ, 127, 2753
Elmegreen B. G., Elmegreen D. M., 1985, ApJ, 288, 438
Eskridge P. B. et al., 2000, AJ, 119, 536
Ferrarese L., Merritt D., 2000, ApJ, 539, L9
Freeman K. C., 1970, ApJ, 160, 811
Friedli D., 1994, in Shlosman I., ed., Mass-Transfer Induced Activity in Galaxies. Cambridge Univ. Press, Cambridge, p. 268
Friedli D., Benz W., 1993, A&A, 268, 65
Gebhardt K. et al., 2000, ApJ, 539, L13
Goodman J., Binney J., 1984, MNRAS, 207, 511
Grosbøl P., Patsis P. A., Pompei E., 2004, A&A, 423, 849
Hasan H., Norman C., 1990, ApJ, 361, 69
Hasan H., Pfenniger D., Norman C., 1993, ApJ, 409, 91
Helfer T. T., Thornley M. D., Regan M. W., Wong T., Sheth K., Vogel S. N., Blitz L., Bock D. C.-J., 2003, ApJS, 145, 259
Heller C. H., Shlosman I., 1994, ApJ, 424, 84
Hernquist L., 1993, ApJS, 86, 389
Hozumi S., Hernquist L., 1998, astro-ph 9806002 (HH)
Hozumi S., Hernquist L., 1999, in Merritt D., Sellwood J. A., Valluri M., eds, ASP Conf. Ser. Vol. 182, Galaxy Dynamics. Astron. Soc. Pac., San Francisco, p. 259 (HH)
Hozumi S., Hernquist L. 2005, PASJ, submitted (HH)
Jogee S., Scoville N., Kenney J., 2005, ApJ, in press (astro-ph/040234)
Kormendy J., Gebhardt K., 2001, in Wheeler J. C., Martel H., eds, AIP Conf. Proc. 586, Relativistic Astrophysics. AIP, New York, p. 363
Kormendy J., Kennicutt R. C., 2004, ARA&A, 42, 603
Kormendy J., Richstone D., 1995, ARA&A, 33, 581
Kuzmin G. G., 1956, Azh, 33, 27
Leeuwin F., Athanassoula E., 2000, MNRAS, 317, 79
McLure R. J., Dunlop J. S., 2002, MNRAS, 331, 795
Magorrian J. et al., 1998, AJ, 115, 2285
Marconi A., Hunt L. K., 2003, ApJ, 589, L21
Monaghan J. J., 1992, ARA&A, 30, 543
Norman C. A., Sellwood J. A., Hasan H., 1996, ApJ, 462, 114 (NSH)
O'Neill J. K., Dubinski J., 2003, MNRAS, 346, 251
Peebles P. J. E., 1972, Ge. Rel. Gravit., 3, 61
Plummer H. C., 1911, MNRAS, 71, 460
Quinlan G. D., Hernquist L., Sigurdsson S., 1995, ApJ, 440, 554
Regan M. W., Teuben P. J., 2004, ApJ, 600, 595
Regan M. W., Thornley M. D., Helfer T. T., Sheth K., Wong T., Vogel S. N., Blitz L., Bock D. C.-J., 2001, ApJ, 561, 218
Sakamoto K., Okumura S. K., Ishizuki S., Scoville N. Z., 1999, ApJ, 525, 691
Sandage A., 1961, The Hubble Atlas of Galaxies. Carnegie Institution, Washington

Schwarz M. P., 1981, ApJ, 247, 77
Seigar M. S., James P. A., 1988, MNRAS, 299, 672
Shapiro S. L., Lightman A. P., 1976, Nat, 262, 743
Shen J., Sellwood J. A., 2004, ApJ, 604, 614 (SS)
Sheth K., Stuart N. V., Regan M. W., Thornley M. D., Teuben P. J., 2005, ApJ, in press (astro-ph/0505393)
Skokos H., Patsis P. A., Athanassoula E., 2002, MNRAS, 333, 847
Toomre A., 1963, ApJ, 138, 385
Toomre A., 1964, ApJ, 139, 1217
Tremaine S. et al., 2002, ApJ, 574, 740
Valenzuela O., Klypin A., 2003, MNRAS, 345, 406
Wada K., Habe A., 1992, MNRAS, 258, 82
Wada K., Habe A., 1995, MNRAS, 277, 433
Young P., 1980, ApJ, 242, 1232

This paper has been typeset from a TEX/LATEX file prepared by the author.